J Mater Sci (2008) 43:5585–5590
DOI 10.1007/s10853-008-2805-9

Enhancement of fiber–matrix adhesion by laser ablation-induced surface microcorrugation

Fahmi Bédoui · N. Sanjeeva Murthy · Frank M. Zimmermann

Received: 29 February 2008 / Accepted: 12 June 2008 / Published online: 8 July 2008

Abstract Micrometer-sized surface corrugations produced on Kevlar fiber surfaces by laser ablation were found to dramatically enhance the mechanical adhesion between the fibers and the epoxy matrix in a fiber-reinforced composite. Symmetric and asymmetric corrugation structures were produced by irradiating the fibers with high-fluence UV laser pulses at various incidence angles. The interfacial shear strength (IFSS) between the fibers and the matrix was measured using the microbond fiber-pullout method. Upon laser ablation treatment, the IFSS increased by 120% with symmetric corrugation profiles obtained with laser irradiation normal to the fiber axis, and 5-fold with asymmetric corrugation profiles obtained with the laser incidence angle at 45° to the fiber axis. A similar enhancement was observed in pullout tests under wet conditions. A simple model based on an elementary analysis of the expected strain field in the presence of interface corrugation is found to provide a quantitative explanation of the observed strength enhancement factors.

Introduction

High-strength fibers are widely used as reinforcements in fiber-reinforced composites to enhance their mechanical properties. The high strength of the fibers and their shape ratio contribute to the increase in the strength under both static and dynamic loading, and also prevent failure. The fiber–matrix adhesion, a key parameter for achieving this goal, is typically improved by electrochemical surface treatments [1], by the use of a specific compatibilizer [2], and by irradiation [3]. In one study, polyethylene fibers were laser-ablated to alter their surface chemistry, resulting in enhanced interfacial shear strength [4, 5]. Here we explore the use of laser ablation to create a rough surface to increase the interfacial shear strength by mechanical interlocking of ablation-induced interface corrugations.

Previous work emphasized the effect of such self-locking in civil engineering materials structures [6]. While laser ablation can be used to produce microstructured surfaces on a relatively small scale, similar structures could be produced on larger scales using scalable methods such as template indentation techniques, with potential applications in many fiber-reinforced materials. Another intriguing potential application of self-locking adhesion due to asymmetric surface corrugations is in the field of surgery, where miniature self-locking sutures could be developed similar to the barbed sutures that have been use for certain surgery application [7].

To quantify the fiber–matrix adhesion, various methods have been used, including single-fiber fragmentation [8], micro-indentation [9], and the microbond or microdebonding technique [10, 11]. The advantages and the disadvantages of the various methods have been summarized by Herrea-Franco and Drzal [12]. The microbond technique seems to be the most appropriate for our application because of its simplicity and acceptable accuracy. This technique consists on pulling a single fiber out of a bead of cured epoxy while measuring the pullout force and displacement. This method has been used with Kevlar 49

F. Bédoui · N. S. Murthy (✉)
New Jersey Center for Biomaterials, Rutgers University, Piscataway, NJ 08854, USA
e-mail: murthy@biology.rutgers.edu

F. M. Zimmermann
Department of Physics and Astronomy and Laboratory for Surface Modification, Rutgers University, Piscataway, NJ 08854, USA

fibers by Miller and Gaur to study the regeneration of adhesive bonding in fiber–resin systems [13]. In this article we present fiber pullout tests data from Kevlar fibers embedded in epoxy to demonstrate the enhancement of fiber–matrix adhesion due to laser-ablated fiber surfaces.

Experimental

Kevlar-29 fibers (DuPont Co.) were chosen for this study because Kevlar is one of the most widely used reinforcing materials in fiber-reinforced composites. The samples were laser-ablated using a frequency-quadrupled Nd:YAG laser with 266 nm wavelength. The pulse energy was measured using a pyroelectric laser power meter. The average pulse fluence was 20 mJ/cm^2. The samples were exposed for 20 s at a pulse repetition rate of 10 Hz. Some fibers were ablated with the laser incidence direction perpendicular to the fiber axis, and others at 45° to the fibers axis.

The surfaces produced upon ablation were examined using a scanning electron microscope (AMRAY 1830 I). Prior to electron microscopy, the samples were sputter coated with gold-palladium using Balzers SCD 004 equipment.

Fiber pullout tests based on the microbond technique [11] were carried out to quantify the effect of ablation on the fiber–matrix adhesion. This technique is based on measuring the force necessary to pull a fiber out of the matrix. An epoxy resin, produced by reacting 4:1 (by weight) mixture of end-capped poly(Bisphenol A-*co*-epichlorohydrin) glycidyl with a curing agent (4,4′-diaminodiphenylmethane), was used as the matrix. A 100–200 μm drop of epoxy was deposited on the Kevlar fiber and cured for 4 h at 75 °C to form a bead. The embedded length and the fiber diameter were measured using an optical microscope (Nikon Optiphot-pol).

A tensile testing machine (MTS, Sintech 5/D) was used to pull a single embedded filament out of the epoxy with the aid of a device shown in Fig. 1a. The fiber was attached to the MTS grip on the top. The epoxy bead was positioned beneath two adjustable blades. The blades were positioned such that they did not contact the fiber but prevented the bead from slipping through between the blades. Pullout tests were performed at a displacement rate of 0.3 mm/min. The effect of water on the fiber–matrix adhesion was studied by soaking the samples (fiber with cured epoxy drop) in tap water for 24 h. The shear stress vs. displacement curve for a typical pullout test is shown in Fig. 1b. An average length of 10 mm was used for all the tested fibers. The large increase in the maximum supported stress in the test with the ablated fiber reflects the increased fiber–matrix adhesion (slope are different probably because of the differences in the size of the epoxy droplet). The effect

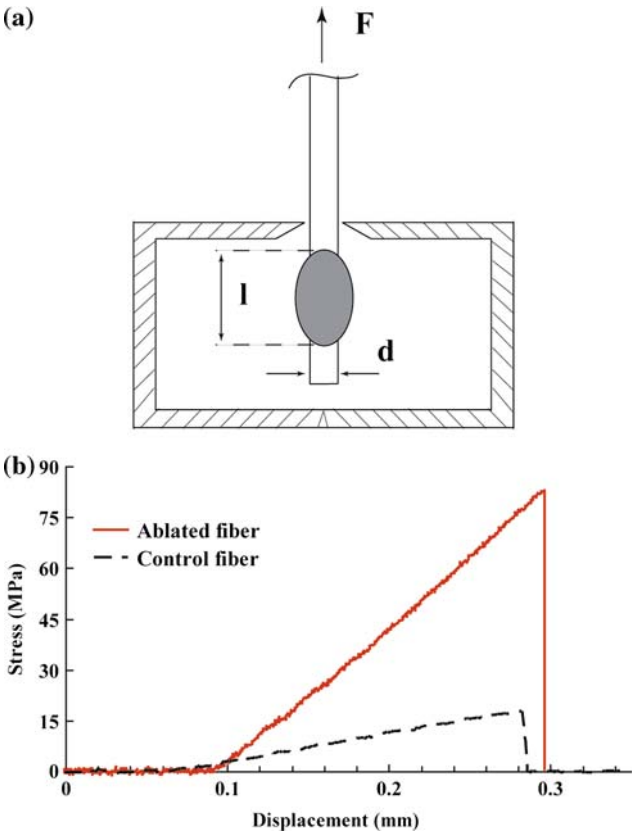

Fig. 1 (**a**) Schematic of the pullout test equipment. (**b**) A typical interfacial shear stress (pullout force normalized to the interface area) vs. displacement curve obtained in a pullout test

of the ablation on the chemical composition of the fiber surface, which could influence the adhesion strength (Fig. 1b), was not studied in this paper.

The interfacial shear strength τ is determined from the maximum force F_{max} using the equation

$$\tau = \frac{F_{max}}{\pi d l} \quad (1)$$

where d is the diameter of the fiber and l is the length of the embedded fiber measured by optical microscopy.

Results

Figure 2 shows some of the morphologies obtained by irradiating Kevlar fibers with UV light from an excimer laser. Such patterns are presumed to be due to the rapid melting and solidification as the polymer fragments are ablated [14]. It is estimated that in strongly UV absorbing polymers such as Kevlar, the thickness of the pool of molten material is about 0.1 μm and the mean temperature gradient is $\sim 6 \times 10^3$ K/μm [15]. Cones and ripples are typically produced when flat surfaces of the polymers in which no orientations are present are irradiated. These

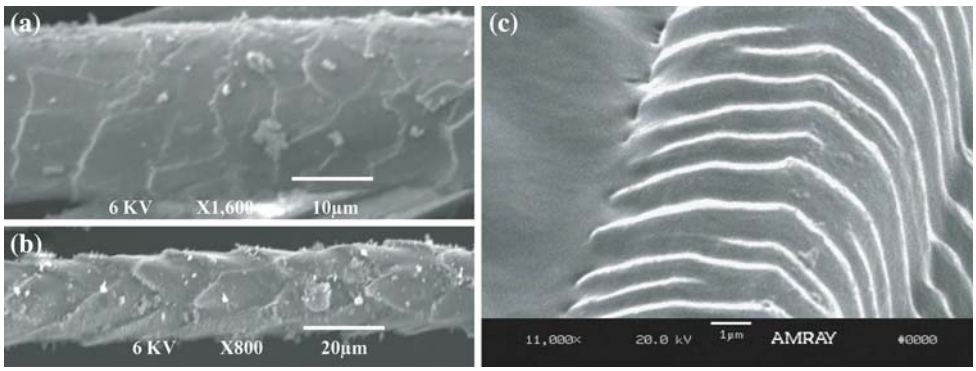

Fig. 2 Different types of structures seen in laser-ablated Kevlar fiber. Structures in (**a**) and (**b**) are similar to Fish scales and were produced using a KrF Excimer UV laser (248 nm). (**c**) Shows one of the corrugated structures investigated in detail in this report; the fiber in this micrograph was ablated with a frequency-quadrupled Nd:YAG laser (266 μm) at 45° incidence

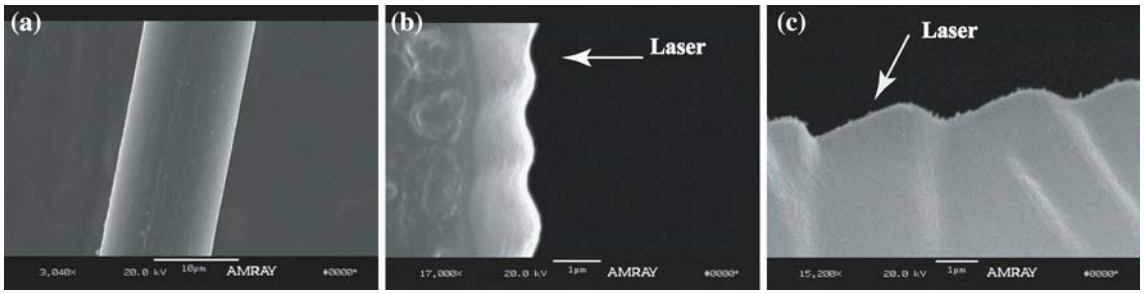

Fig. 3 Scanning electron micrographs of ablated surfaces of Kevlar fibers. (**a**) Control fiber; (**b**) Ablated fiber with the laser perpendicular to the fiber; and (**c**) Ablated fiber with the fiber axis at 45° relative to direction of the laser. The fiber in these micrographs were ablated with a frequency-quadrupled Nd:YAG laser (266 μm)

features are explained by invoking Marangoni convection that result from instabilities as a result of local temperature fluctuations [14]. When the local temperature on the free surface is higher than the equilibrium temperature, its surface tension decreases, and the surrounding cooler regions with a higher surface tension pull the liquid away. As the melt is ejected radially from the heated region to the colder regions, to preserve mass, hot fluid ascends from the lower plane. A system of Marangoni cells is thus develops wherein fluid ascends near the center of the cells and descends around the periphery. In addition to these considerations, in the case of fibers we must take into account the fact that in fibers, the polymer chains are highly oriented and are under considerable internal stresses. When the highly stressed layer is melted, in addition to convective instabilities due to viscosity gradients perpendicular to the surface, we expect lateral instabilities as the polymer chains recoil and the internal stresses are released in the molten layer. Comparing the images [16] shown in Fig. 2 with those of Bahners and Schollmeyer [15] and Yip et al. [17], it is evident that the patterns obtained from drawn fibers are quite different from those obtained from isotropic films. The scale-like structures that are observed are thought to be due to coupling of thermal and mechanical fields [15]. Different patterns such as the ones shown in Fig. 2 may arise depending on which of the mechanisms, temperature- or and stress-induced instabilities, dominate the melting and solidification process.

Figure 3 shows scanning electron micrographs (SEM) of ablated surfaces of Kevlar fibers. When the laser pulses impinged on the surface perpendicular to the fiber axis, symmetrical ripples were produced, with a depth of approximately 0.25 μm and a periodicity of approx. 1.5 μm (Fig. 3b). When the laser pulses impinged on the surface at an angle of 45° with respect to the fiber axis, the ripples had a saw-tooth-like waveform with a depth of approx. 0.5 μm and a periodicity of approx. 3 μm (Fig. 3c). Morphologies similar to the symmetric corrugations observed here have been produced by laser ablation of nylon fibers [15, 17] and widow spider silk [16]. These ripples were erased by a second ablation at an angle of 70° resulting in a smooth ablated surface [16].

Pullout tests were carried out in both directions to measure the effect of the self-locking feature due to the asymmetry of the ripples. The adhesion increased by about 120% in 90°-ablated fibers under dry condition (Fig. 4). In the 45°-ablated fibers, the adhesion increased by 90% when the fiber was pulled along the ripples as shown in Fig. 4, and about five-fold when the fiber was pulled against the ripple direction. Figure 5 shows the result for the adhesion in the case of the ablated fibers with laser incidence angle of 45°, pulled out in the direction opposite to that of

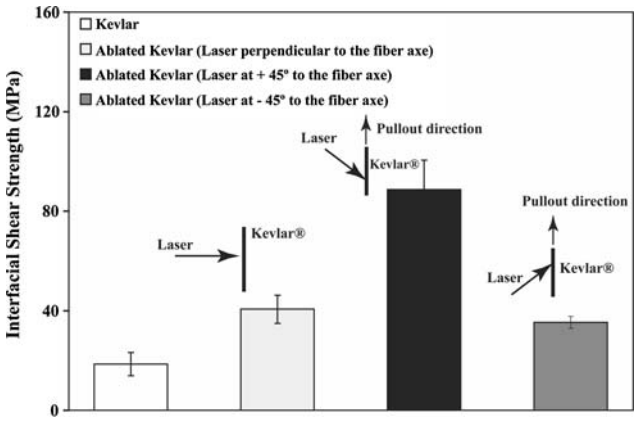

Fig. 4 Comparison of the interfacial shears strengths of the ablated and unablated under wet conditions. Fibers with cured epoxy beads were immersed in water for 24 h prior to the pullout tests

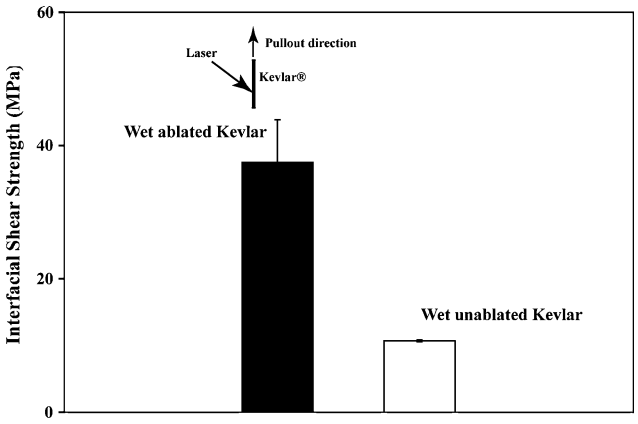

Fig. 5 Comparison of the interfacial shears strengths of the ablated and unablated fibers under dry conditions

ablation, after immersion in water for 24 h. Under wet conditions, the adhesion strength for the ablated fibers was four times as large as for the wet, unablated controls, and still twice as large as for the unablated fibers under dry conditions.

Figure 6 presents a comparison between ablated fiber surfaces before and after the pullout tests, for two different fibers. In the post-pullout micrograph, the corrugations are still visible, but they appear to have been abraded, and abraded matrix material appears to be present in some of the troughs of the corrugation. We note that while valuable, images like Fig. 6b do not give direct clues about the initial failure mechanism, since the violent pullout process subsequent to initial failure, which is associated with large frictional forces and frictional heating, may result in the observed abrasion, while the initial failure was in fact interfacial debonding.

The adhesion is expected to be stronger with ablated fibers that have surface corrugations than with smooth, unablated fibers because of the larger surface area, and because the saw-tooth-like profile is intuitively expected to produce an additional self-locking effect, which we model below. The observed asymmetry in the shear strength could potentially be exploited in a self-locking suture, which would offer little resistance to insertion, but the asymmetric ripples would prevent the fiber from slipping back out.

Model

While a realistic description of the stress and strain fields and the debonding mechanics in a fiber pullout experiment requires sophisticated analytical or numerical techniques [18–20], we have found that a very simple model is sufficient to explain the observed strength enhancement and its dependence on the corrugation topography and asymmetry with respect to pullout direction in laser corrugated fibers. Despite the model's simplifications, we believe that it captures the essential physics involved.

We begin with a fiber of radius r embedded in a matrix, with a pulling force F applied in the axial direction. The force gives rise to a shear stress near the interface of magnitude $\sigma_0 = \Delta F/2\pi r\Delta l$, where $\Delta F/\Delta l$ is the force per unit length at a given position along the fiber. This shear stress is expected to vary along the length of the fiber due to elastic deformation of the fiber and the matrix. We focus our attention on a particular spot along the fiber where the

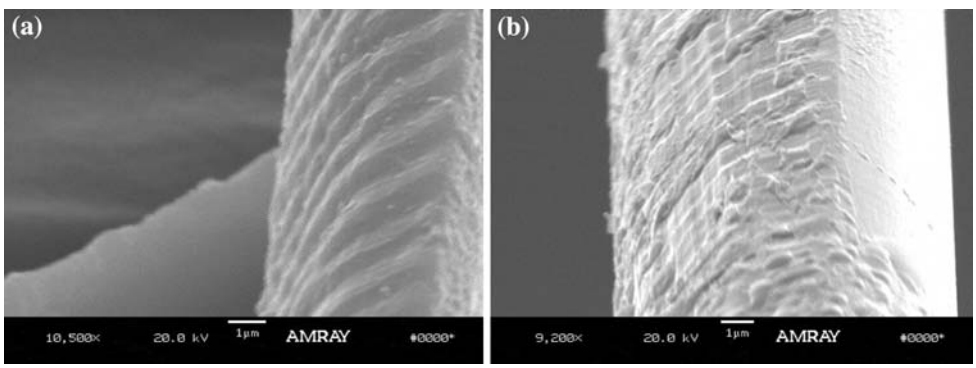

Fig. 6 Scanning electron micrographs of: (**a**) the control ablated fiber before the pullout test and (**b**) the ablated fiber surface after pullout test

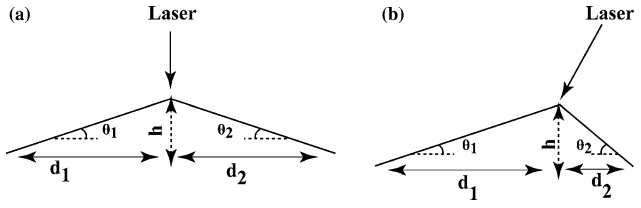

Fig. 7 Schematic representation of the corrugation morphology depending on the laser incidence

applied shear stress σ_0 should be considered as the independent variable. For a smooth fiber, debonding will occur when the applied stress σ_0 exceeds the interfacial shear strength $Z_\parallel$.

To derive an expression for the maximum supported shear stress in the presence of laser-induced interface corrugation, we first approximate the observed corrugation profiles (Fig. 3) as a symmetric or asymmetric triangular wave with a rising portion d_1 and a falling portion d_2 and a peak-to-trough height h as shown schematically in Fig. 7. By fitting such idealized triangular waves to the profiles of Fig. 2, we estimate the aspect ratio of the fitted triangular profile $\gamma = (d_1 + d_2)/h \approx 4.5$ for both the symmetric and asymmetric corrugations. The asymmetry of the corrugation may be quantified by the asymmetry parameter $a = (d_1 - d_2)/(d_1 + d_2)$. From Fig. 3b, we estimate that $a = 0$ for normal laser incidence, while $a \approx +1/3$ in Fig. 3c for oblique incidence ablation. The reversed profile, resulting from the laser beam tilted the other way, then corresponds to a negative asymmetry parameter, $a \approx -1/3$. With the model interface geometry thus defined, we may express the local interface tilt angles (with respect to the fiber axis) via $\tan\theta_1 = h/d_1$ and $\tan\theta_2 = h/d_2$ for the rising and falling portions of the profile, respectively.

In our (simplified) model, the applied pulling force along the x-axis is thought to give rise to a uniform stress tensor $\boldsymbol{\sigma}$ near the interface with shear components $\sigma_{xy} = \sigma_{yx} = \sigma_0$, while all other components are zero. (We have placed the x-axis along the fiber axis, and the y-axis perpendicular to the interface plane, averaged over corrugations.) If the microscopic interface has a local tilt angle θ with respect to the fiber axis, with an interface normal unit vector $\hat{\mathbf{n}} = (\sin\theta, \cos\theta, 0)$, the force vector (per unit area) acting on the interface is given by $\mathbf{s} = \boldsymbol{\sigma} \cdot \hat{\mathbf{n}} = (\sigma_0 \cos\theta, \sigma_0 \sin\theta, 0)$. The component of this force vector perpendicular to the interface (along $\hat{\mathbf{n}}$) has magnitude $s_\perp = \hat{\mathbf{n}} \cdot \mathbf{s} = 2\sigma_0 \sin\theta\cos\theta$, while the component parallel to the interface $\mathbf{s}_\parallel = \mathbf{s} - s_\perp \hat{\mathbf{n}}$ has magnitude $s_\parallel = \sigma_0(\cos^2\theta - \sin^2\theta)$ A simple delamination criterion that accounts for weakening of the interfacial shear strength due to tensile normal stress, and strengthening of the interfacial shear strength due to compressive normal stress is given by [21, 22]

$$\left(\frac{s_\parallel}{Z_\parallel}\right)^2 - \frac{s_\perp}{Z_\perp} = 1 \tag{2}$$

where $Z_\parallel$ is the shear debonding strength (in the absence of normal stress), and $Z_\perp$ is the normal (tensile) debonding strength (in the absence of shear stress).[1] Equation 2 results from the quadratic stress criterion of Kim and Soni [21] for infinite compressive strength ($z' \to \infty$ in the notation of Kim and Soni [21]). The minus sign in Eq. 2 reflects our sign convention of $s_\perp > 0$ for compression, and $s_\perp < 0$ for tension. Applying this criterion to the perpendicular and parallel interface force components of our model, and solving for the maximum applied pulling stress σ_0, we obtain $\sigma_c = Z_\parallel\left(\sqrt{p^2 + 4q} + p\right)\Big/2q$, with $q = (\cos^2\theta - \sin^2\theta)^2$ and $p = 2\left(Z_\parallel/Z_\perp\right)\sin\theta\cos\theta$. The above result applies if the surface tilt is in the direction of the pulling force, i.e., the normal component of the surface force is compressive. In the opposite tilt geometry, if the normal component is tensile, the maximum supported pulling strain is $\sigma_t = Z_\parallel\left(\sqrt{p^2 + 4q} - p\right)\Big/2q$. As one would expect, the model predicts that the debonding strength in the compressive case is enhanced compared to the uncorrugated surface, while the debonding strength is weakened in the tensile geometry. As we increase the applied stress in the fiber pullout experiment, the stress thus exceeds the (weakened) debonding limit in the tensile regions first, upon which the tensile regions are thought to debond. However, this does not lead to failure since the compressive regions are still stressed considerably below their (corrugation-enhanced) debonding strength. The applied force, however, at this time no longer remains uniformly distributed among the tensile and compressive regions, but becomes concentrated on the compressive regions of length d_2, leading to an enhancement of the local shear stress in the compressive regions by a factor of $(d_1 + d_2)/d_2$. The failure criterion thus becomes $\sigma_{fail} = \sigma_c d_2/(d_1 + d_2)$. In Fig. 8 we have plotted the predicted strength enhancement, $\sigma_{fail}/Z_\parallel$, as a function of asymmetry parameter, for the observed aspect ratio $\gamma = 4.5$ and $Z_\parallel/Z_\perp = 2.2$. The experimentally observed strength enhancement is also plotted in the figure, for the three observed asymmetry parameters of $-1/3$, 0, and $+1/3$. Evidently, the simple model can satisfactorily explain the observed strength enhancement factors, and their asymmetry. The only parameter in the model, which was not known, and was thus adjusted to optimize the fit to the data, is the interface strength ratio $Z_\parallel/Z_\perp$. The obtained value of 2.2 is within

[1] Equation 2, solved for $s_\perp$, may be interpreted as the power series expansion of the exact (but unknown) dependence of the normal interface strength $s_\perp$ on the applied shear stress $s_\parallel$ up to second order in $s_\parallel$. Since a reversal of the sign of $s_\parallel$ should have no effect on the perpendicular strength, $s_\perp$ is an even function of $s_\parallel$, i.e., the linear term in the power series expansion vanishes.

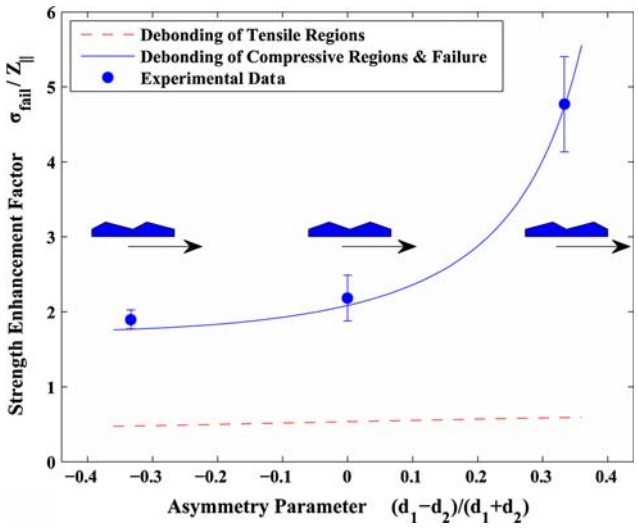

Fig. 8 Calculated strength enhancement factor of ablated fibers, compared to non-ablated fibers, as a function of corrugation asymmetry, using the theoretical model presented in the text. The measured data points are plotted as solid circles. The insets show the interface geometries considered in the model, as well as the pullout direction (*arrow*), corresponding to the three asymmetry parameters for which pullout experiments were performed

the range of values (ranging from 1.63 to 2.25) measured by Brewer and Lagace for graphite fiber/epoxy laminates [22]. In light of this numerical agreement (albeit for different interfaces), the fitted value appears physically reasonable.

Conclusion

The interfacial shear strength of the fiber–matrix composites increases dramatically when surface microcorrugations are created on the fiber surface by laser ablation. A simple model based on mechanical interlocking explains the enhancement. Large strength enhancement factors persist even in the presence of water that weakens the interfacial shear strength. Thus, this laser ablation technique could be a useful method to strengthen the fiber–matrix adhesion in the presence of solvents that degrade adhesion. The shape and symmetry of the created surface corrugations can be controlled by the angle of incidence of the laser beam relative to the fiber axis. A 45° incidence angle produces an asymmetric saw-tooth-like profile that due to mechanical self-locking enhances the shear strength in one direction by a much greater factor than in the other direction.

Acknowledgements The authors acknowledge Y. Kamath for helpful discussions on the experimental aspect of the pullout tests and R. Govinthasamy for preliminary work on this project. The study was funded by the National Science Foundation under award # DMR-0513926.

References

1. King JA, Buttry DA, Adams DF (1993) Polym Compos 14:301. doi:10.1002/pc.750140405
2. Manchado MAL, Arroyo M, Bagiotti J, Kenny JM (2003) J Appl Polym Sci 90:2170. doi:10.1002/app.12866
3. Xu Z, Huang Y, Zhang C, Liu L, Zhang Y, Wang L (2007) Compos Sci Technol 67:3261
4. Song Q, Netravali AN (1998) J Adhes Sci Technol 12:957. doi:10.1163/156856198X00579
5. Song Q, Netravali AN (1999) J Adhes Sci Technol 13:501. doi:10.1163/156856199X00064
6. Tastani SP, Pantazopoulou SJ (2002) In: Bond in concrete—from research to standards, Publication of CEB-FIP, ACI and JCI, Budapest, Hungary, November 2002, pp 1–8
7. Ebert EA (1992) US Patent 5127413
8. Zhou XF, Nairn JA, Wagner HD (1999) Composites Part A 30:1387. doi:10.1016/S1359-835X(99)00043-3
9. Tsukamoto Y, Kuroda H, Sato A, Yamaguchi H (1992) Thin Solid Films Switz 213:220. doi:10.1016/0040-6090(92)90285-J
10. Mandell JF, Chen JH, McGarry FJ (1980) Int J Adhes Adhes 1:40. doi:10.1016/0143-7496(80)90033-0
11. Miller B, Muri P, Rebenfeld L (1987) Compos Sci Technol 28:17. doi:10.1016/0266-3538(87)90059-5
12. Herrera-Franco PJ, Drzal LT (1992) Composites 23:2. doi:10.1016/0010-4361(92)90282-Y
13. Miller B, Gaur U (1989) J Adhes 29:103. doi:10.1080/00218468908026480
14. Murthy NS, Prabhu RD, Martin JJ, Zhou L, Headrick RL (2006) J Appl Phys 100(023538):1
15. Bahners T, Schollmeyer E (1989) J Appl Phys 66:1884. doi:10.1063/1.344371
16. Moore A, Koch M, Mueller K, Stuke M (2003) Appl Phys A 77:353. doi:10.1007/s00339-003-2193-6
17. Yip J, Chan K, Sin KM, Lau KS (2004) Polym Int 53:627. doi:10.1002/pi.1420
18. Hsueh CH (1992) Mater Sci Eng A 154:125. doi:10.1016/0921-5093(92)90337-Z
19. Yue CY, Cheng WL (1992) J Mater Sci 27:3173. doi:10.1007/BF01116007
20. Zhou LM, Kim JK, Mai YW (1992) Compos Sci Technol 45:153. doi:10.1016/0266-3538(92)90037-4
21. Kim RY, Soni SR (1986) In: Kawata K, Umekawa S, Kobayashi A (eds) Composites '86: recent advances in Japan and the United States, Proc. Japan-U.S. CCM-III, Tokyo, pp 341–350
22. Brewer JC, Lagace PA (1988) J Compos Mater 22:1141. doi:10.1177/002199838802201205